Visual Neuroscience (2008), **25**, 179–185. Printed in the USA.

doi: 10.1017/S0952523808080413

Foveal evoked magneto-encephalography features related to the parvocellular pathway

CHIA-YEN YANG,[1] JEN-CHUEN HSIEH,[2,3,4,5] AND YIN CHANG[1]

[1]Institute of Biomedical Engineering, National Yang-Ming University, Taipei, Taiwan, Republic of China
[2]Institute of Health Informatics and Decision Making, School of Medicine, National Yang-Ming University, Taipei, Taiwan, Republic of China
[3]Institute of Neuroscience, School of Life Science, National Yang-Ming University, Taipei, Taiwan, Republic of China
[4]Faculty of Medicine, School of Medicine, National Yang-Ming University, Taipei, Taiwan, Republic of China
[5]Laboratory of Integrated Brain Research, Department of Medical Research and Education, Taipei Veterans General Hospital, Taipei, Taiwan, Republic of China

(RECEIVED June 25, 2007; ACCEPTED February 14, 2008)

Abstract

The aim of this study was to use non-invasive magneto-encephalographic techniques, together with visual stimulus paradigms that can psychophysically separate the M- and P-pathways, to examine the physiological relations of the pathways at the fovea with (1) the magneto-encephalography components M70 and M100 (in latency and amplitude), and (2) the cortical oscillatory activities (alpha, beta, and gamma), respectively. The checkerboard stimuli accompanied with different spatial frequencies (SFs) (0.5 or 4 cycles per degree) were presented (within 2° of the retinal center) to six healthy subjects by using steady-pedestal and pulse paradigms, which could activate distinct populations of M- and P-neurons. SF analyzed brain responses in each paradigm. The results show a consistent trend in M70 and M100 with increased latencies and amplitudes in response to the high SF. Mean while, the beta to gamma activities are apparently enhanced by the stimulus of high SF, especially under pulse paradigm ($p = 0.03$). In this study, we suggest that M70 can be a good clue to characterize the P-pathway. Moreover, in the frequency analysis, the beta oscillations may serve for more detailed visual information, while the gamma oscillations seem to reflect the signal processing in the P-pathway and with sensitivity to the fovea.

Keywords: Parvocellular, Spatial frequency, Fovea; Wavelet, Magneto-encephalograph

Introduction

Foveal vision is used for scrutinizing the most detail and extensive information about the environment. With such visual acuity, this central part of the retina plays an important role in perception. It has been well known that visual signals beginning in the retina of the primate visual system are conveyed along both the parvo- (P-) and the magno-cellular (M-) pathways (Merigan et al., 1993; Schwartz, 1999; Bear et al., 2001; Purves et al., 2001). In several aspects, there are essential differences between these two pathways. Morphologically, somas of P-cells have smaller diameters and dendritic fields than those of M-cells. Physiologically, signals propagate more slowly in P-cells than those in M-cells. In response to stimulus, P-cells have sustained responses and can resolve lower temporal frequencies, whereas M-cells are just the opposite (transient responses and higher temporal frequencies). Functionally, P-cells can carry information associated with color but have lower luminance contrast sensitivity. On the contrary, M-cells have higher contrast sensitivity over a wide range of luminance (Schiller et al., 1991; Arakawa et al., 1999).

Psychophysical studies have demonstrated that the spatial frequency (SF) responses carried in the P- and M-pathways can be distinguished by stimuli of different temporal waveforms (e.g., Wilson, 1978). Wilson et al. (1983) reported that there are specialized neural channels to analyze the SF contents of visual stimuli. Kenemans et al. (2000) also showed that a relatively strong activation in the secondary (lateral occipital) areas could be elicited by low SFs (<1 cycle per degree (cpd)), whereas a relatively strong activation in the primary (medial occipital) areas could be elicited by high SFs (>4 cpd). Those particular spatial-frequency-sensitive areas might relate to the M- and P-pathways. Studies using electroencephalography (EEG) (Proverbio et al., 1996) and magneto-encephalography (MEG) (Tzelepi et al., 2001) suggest that the N70 component (a negative peak around 70 ms) is sensitive to SF change, similar to the human contrast sensitivity function with peak amplitude at about 4 cpd (Wilson et al., 1983). However, the P100 (a positive peak around 100 ms) has also been considered to carry characteristics of both pathways (Baseler & Sutter, 1997; Reed et al., 1984; Tobimatsu et al., 1995).

Address correspondence and reprint requests to: Yin Chang, Institute of Biomedical Engineering, National Yang-Ming University, 155 Section 2 Li-Nong Street, Shih-Pai, Peitou, Taipei 112, Taiwan, Republic of China. E-mail: ychang@bme.ym.edu.tw

Rhythmic oscillations in EEG have been considered to reflect dynamic changes in intrinsic brain activity (Basar et al., 2001; Adeli et al., 2003). Visual studies in both humans (Tallon-Baudry & Bertrand, 1999; Tzelepi et al., 2000; Basar et al., 2001; Karakas et al., 2001; Sakowitz et al., 2001; Varela et al., 2001; Lee et al., 2003) and non-human primates (Eckhorn et al., 1993; Kruse & Eckhorn, 1996) have indicated that high-frequency oscillatory potentials (>30 Hz) evoked by visual stimulation are associated with information processing, perception, learning, and cognitive tasks. Hence, in addition to observing waveforms in the time domain, information in the frequency domain (especially in the beta and gamma bands) is also worth examining. Therefore, we try to use MEG techniques, along with visual stimulus paradigms, which have been successfully used to separate the M- and P-pathways psychophysically (Pokorny & Smith, 1997; Leonova et al., 2003), to examine the relations of the two pathways at the fovea with (1) the MEG components M70 and M100 (latency and amplitude), and (2) the cortical oscillatory activities (theta, alpha, beta, and gamma), respectively.

Materials and methods

Subjects

Six healthy right-handed subjects (four males and two females, all ophthalmically and neurologically normal) were recruited in this study. Their ages ranged from 23 to 26 years (24.2 ± 1.2 years, mean ± SD). The visual acuity of all subjects was, after correction, better than 20/25. Informed consent was obtained from all participants after the experiment was fully described to them.

Visual stimuli and stimulation procedure

In order to separately stimulate the M- and P-pathways in the retina, the stimulus paradigms used in this study were a modifications of that employed by Pokorny and Smith (1997) and Leonova et al. (2003). Their psychophysical data demonstrated that both pathways have different temporal contrast gains: the M-pathway has very high sensitivity to the contrast change whereas the P-pathway does not. For the steady-pedestal paradigm, the pedestal was presented continuously and for the pulse paradigm, the pedestal was only presented in the stimulus interval. The idea behind such presentation was that the pedestal in the pulse paradigm was designed to desensitize the magnocellular pathway that is very sensitive to the rapid luminance changes—in that case, the parvocellular pathway would determine the contrast detection. Thus, temporal changes in background luminance were intended either to stimulate the M-pathway (steady-pedestal paradigm) or to saturate it and allow the P-pathway to react to the pattern stimulus (pulse paradigm) (Plainis & Murray, 2005).

The stimulus was a radial checkerboard, or a dartboard-like pattern presented in black and white with an average luminance of 6.0 cd/m^2 on a homogeneous gray pedestal (size = 19.2° × 19.2°), against a uniform background (size = 31.8° × 23.8° with an average luminance of 1.0 cd/m^2). The field size of the stimuli was 2° in radius. As considering cortical magnification factor, stimulus patches increased their size linearly with eccentricity. To or not to further desensitize the P-pathway, the pattern contrast was set at 33% or 94% (Michelson fraction), respectively. The corresponding stimulus paradigms are shown in Figs. 1a and 1b. Two fundamental SFs (0.5 and 4 cpd) of the checkerboard were randomly chosen. Thus, four test tasks were formed the two variables of SF and stimulus paradigm.

The stimulation procedure was as follows. Under the condition of steady-pedestal (Fig. 1a) the subject first adapted to the background—a dimly lit screen (1 cd/m^2) plus a pedestal (6 cd/m^2)—for 1 min and then the stimulus was given. During the trial, the duration of the stimulus was a constant 50 ms and the stimulus onset asynchrony was varied between 550 and 1000 ms to

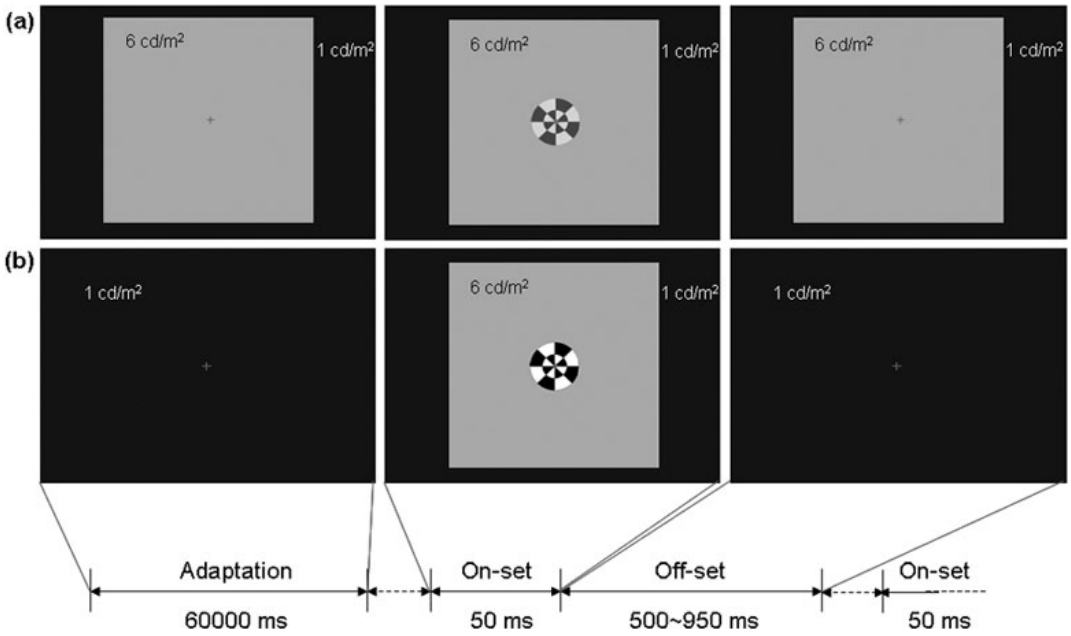

Fig. 1. Two types of stimulus paradigms applied to the foveal region. (**a**) The steady-pedestal paradigm. (**b**) The pulse paradigm. In this case, subject adapted to the background for 1 min followed by the stimulus pattern with low SF of 0.5 cpd—a radial checkerboard—in an alternate ON-OFF mode. The time course of presentation is shown. (The dotted arrow indicates a stimulus onset variability, which varied randomly from 0 to 450 ms.)

avoid adaptation problems. The background luminance was held constant between trials. Similarly, under the pulse condition (Fig. 1b); the stimulation procedure was the same as the steady-pedestal, except the "off-set" part of the stimulus pattern was changed to a dim background without the pedestal. Stimuli were generated with a personal computer, using Presentation software (v. 0.55, Neurobehavioral Systems, Inc., Albany, CA) and projected onto a transparent screen by a projector (Electrohome Electronics 38-DM0001-EXP, Ontario, Canada). The pattern was viewed binocularly at a distance of 120 cm from the screen. A small red cross ($35'' \times 35''$) was provided in the central field for eye fixation.

Measurement

Visual evoked fields were recorded with a whole-head 306-channel neuromagnetometer (Vectorview, 4-D Neuroimaging, San Diego, CA). Horizontally and vertically bipolar electrooculograms (EOGs) were recorded at the same time as the magnetic-field data. Artifact rejection was performed by removing epochs with amplitudes exceeding 6000 f T/cm in the MEG or 300 uV in the EOG signals. The magnetic responses were filtered by a 0.1–200 Hz bandpass filter and digitized at a sampling rate of 512 Hz. The delay time between the generation of trigger pulses from the computer and the display of patterns from the projector was measured by a photodiode attached to the screen; for off-line analysis of the data (which were recorded between 100 ms before and up to 500 ms after the stimuli), the average time was shifted 35 ms due to this delay. One hundred epochs were averaged for each session. The mean signal level in the prestimulus period (100 ms) was defined as the baseline and treated as a DC offset. Procedures of co-registration of MEG and MRI are published elsewhere (Yang et al., 2006).

Data analysis

Source analysis

The equivalent current dipole (ECD) model in a spherical volume was used to estimate the apparent source of cortical activity. The location of the source (x, y, z) and the orientation of the intensity of the dipole (Qx, Qy, Qz) were fitted to the conventional head-based x-y-z coordinate system (toward the right preauricular point, the nasion, and the head vertex, respectively). To identify the sources of the measured signals, deflections around the occipital area were first visually searched to select the time windows. During these time windows (i.e., 60–80 ms for M70 and 80–120 ms for M100), a moving dipole was applied to fit the magnetic fields at each time sample. If the goodness of fit (GOF) was not more than 80% for the dipole fitting of the whole head, the boundary of the estimated region of interest was restricted to the occipital area, a subset of channels (at least 30). The initial estimation was identified by its GOF and anatomic site. Thereafter, the ECD with the best description of the measured signals was found. When a single ECD is not able to appropriately fit the occipital pole source due to intrinsic variability (Odaka et al., 1996), two-dipole model was then employed. The criteria used to ensure a good dipole fitting was the ECDs accounting for more than 85% of the GOF value.

Wavelet analysis

The wavelet analysis was used to extract more information in both the time and frequency domains. This method has the advantage of giving good time resolution in the high-frequency band and good frequency resolution in the low-frequency band (Quiroga & Schürmann, 1999; Samar et al., 1999). The Morlet wavelet of order seven was employed in this study (Kronland-Martinet et al., 1987). In order to reduce the amplitude of spontaneous oscillatory activity, trials were averaged and then subjected to wavelet transformation. Meanwhile, the signal space projection (SSP) method was also used to remove environmental interferences from the weak magnetic signals (Taulu et al., 2005). The time-frequency maps (time varying power for each frequency, f_0) were then constructed by squaring the convolution of the SSP-cleaned and averaged signal $\bar{x}(t)$ with the Morlet complex mother wavelet $\psi(t, f_0)$:

$$WTavg(t, f_0) = |\psi(t, f_0) * \bar{x}(t)|^2,$$

where

$$\psi(t, f_0) = A \exp(-t^2/2\sigma_t^2)\exp(i2\pi f_0 t),$$

$$A = 1/(\sigma_t\sqrt{2\pi}),$$

$$\sigma_t = 1/(2\pi\sigma_f),$$

and

$$\bar{x}(t) = \frac{1}{n}\sum_{i=1}^{n} x_i(t).$$

The mean time-frequency representation was calculated from two or three MEG channels showing the strongest power over the occipital region. (To verify the validity of using sensor-based signals, the beta-range activities of the time-frequency maps were chosen for source localization as examination. The locations of ECDs overlaid on standard MRIs were near the calcarin fissure with a mean coordinate at (-5.90 ± 8.77, -87.23 ± 6.13, 6.79 ± 3.29) in Talairach coordinate.) These data were then baseline-corrected by subtracting the mean power prior to the stimulus onset (-100 to 0 ms) for each time point. After that, each power map was screened into several frequency bands by using the threshold, which is defined as half of the maximum value (half power), for further statistical analysis. (Under the steady-pedestal paradigm, three frequency bands were evaluated: 3–6 Hz for theta, 7–12 Hz for alpha and 13–25 Hz for beta; under the pulse paradigm, five frequency bands were evaluated: 3–7 Hz for theta, 8–13 Hz for alpha, 14–18 Hz for beta 1, 19–25 Hz for beta 2, and 26–36 Hz for gamma. The choice of frequency bands was determined individually from the threshold, which is defined as half of the maximum value in every time-frequency map.)

Statistics

Two-tailed Wilcoxon signed-rank test (nonparametric statistics) was applied to analyze the responses between low and high SFs in each paradigm. The difference was taken as significant when the probability value (p) was less than 0.05. All measured quantitative values are presented by mean and standard deviation.

Results

Figs. 2a and 2b show the topographic distribution of the magnetic responses from Subject 6 with respect to different SFs in the steady-pedestal and pulse paradigms, respectively. The intensity

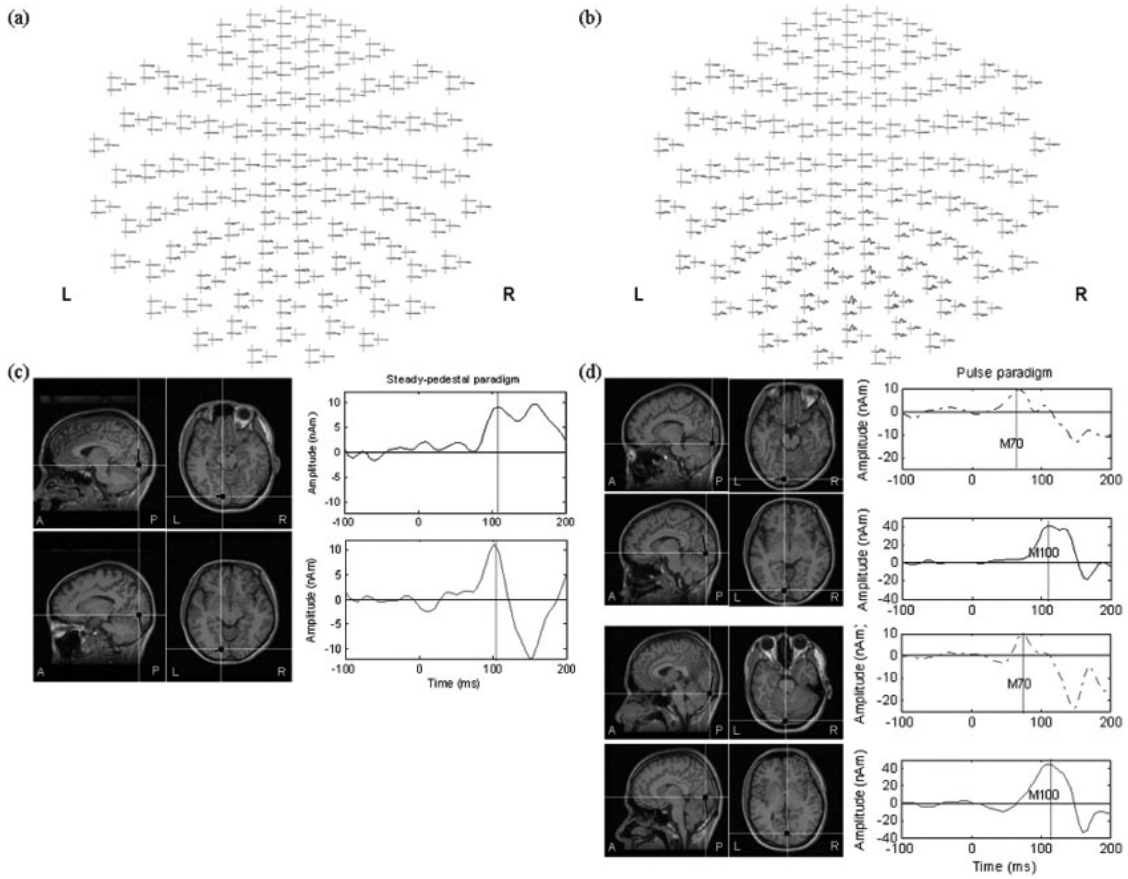

Fig. 2. (**a**) and (**b**) Topographic distribution of the magnetic responses from Subject 6 to different SFs in steady-pedestal and pulse paradigms. The head is flatten to a plane and viewed from the top. (**c**) One-dipole fitting for M100 under the steady-pedestal paradigm. (**d**) Two-dipole fitting for M70 and M100 under the pulse paradigm. **Left**: locations of the ECDs superimposed on Subject 6's MR images. **Right**: waveforms of the ECDs as a function of time. In all plots, the panels of upper one in Fig. 2c and upper two in Fig. 2d represent responses to the low SF, while the panels of lower one in Fig. 2c and lower two in Fig. 2d represent responses to the high SF.

waveforms of their ECDs were shown in Figs. 2c and 2d, correspondingly. A one-dipole source model was used to fit the M100 responses under the steady-pedestal paradigm, whereas a two-dipole source model was applied for the M70 and M100 responses under the pulse paradigm. In all plots, the panels of upper one in Fig. 2c and upper two in Fig. 2d represent the responses to the low SF, the panels of lower one in Fig. 2c and lower two in Fig. 2d are for the high SF. The locations of ECDs were overlaid on MRIs and all found to be nearby the calcarin fissure.

Statistical analysis associated with latency and intensity of the dipole waveforms for M70 and M100 components are shown in Fig. 3. No significant difference ($p > 0.05$) is revealed in the analysis between low and high SFs produced by each paradigm of test tasks. However, the increased mean value in each category from low SF to high SF is observed.

Fig. 4 shows the time-frequency representation of the magnetic responses from Subject 3 to different SFs in steady-pedestal and pulse paradigms. The upper panels are responses to the low SF; the lower ones are for the high SF. The magnitude of spectral power (T^2/cm^2) from low to high is indicated by colors from blue to red. The signals are presented over a time course of -100 to 500 ms and the plots are displayed in terms of frequency versus time.

The power distributions in each frequency band were compared to each other over time (Fig. 5). The results can be summarized as follows. First, within the theta and alpha bands, the power was stronger to the stimulus of low SF than to the high SF stimulated by steady-pedestal paradigm and stronger to the stimulus of high SF than to the low SF driven by pulse paradigm. However, no significance was found between the responses elicited by different SFs (all $p > 0.05$). Second, within the beta band, the power was stronger to the stimulus of high SF than to the low SF stimulated by steady-pedestal paradigm, in which significant differences were explicitly revealed within 0–124 ms (all $p < 0.03$). Meanwhile, similar results in statistical test also occurred around 100 ms with $p = 0.03$ in the beta 2 band under the stimuli of pulse paradigm. Third, within the gamma band, the power was stronger to the stimulus of high SF than to the low SF stimulated by pulse paradigm. Statistically significant differences were apparently shown between the responses stimulated by different SFs right after the stimulus pattern onset (all $p < 0.05$).

Discussion

It is generally agreed that magnocellular retinal ganglion cells have large cell bodies and dendritic fields, whereas parvocellular retinal ganglion cells are just the opposite (small bodies and fields). The peak latency of the visual evoked response should relate to the neural circuitry and the physiological properties of the cell types.

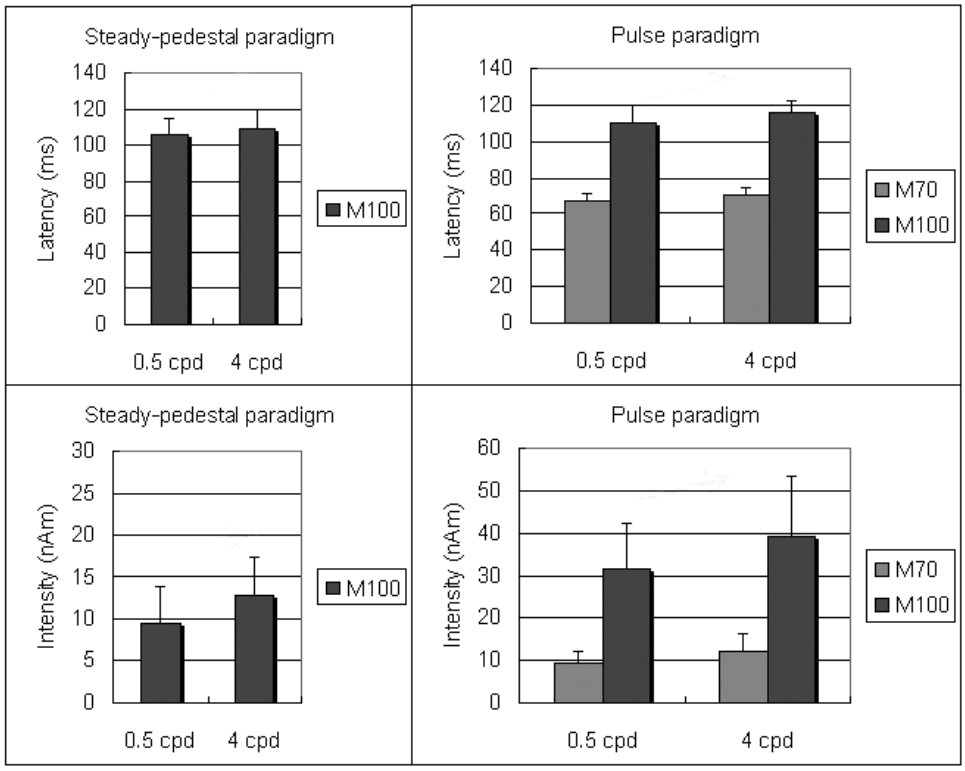

Fig. 3. Mean peak latencies and dipole intensities of M100 and/or M70 responses across subjects under steady-pedestal and pulse paradigms. Even though no statistically significant difference is revealed in the analysis ($0.05 < p < 0.1$) between low and high SFs produced by each paradigm of test tasks, however, the amplitude or latency of each component seems to incline with increasing SF.

Our results showed that, for the M70 component, latencies increased with high SF and similar to the M100 component. The latency measurements in both M- and P-conditions (by using steady-pedestal and pulse paradigms, respectively) were similar to the study of Tzelepi et al. (2001), which showed that the N70m latency difference between 1 cpd and 3 cpd was about 3–6 ms. According to the VEP study of Jones and Blume (2000), the median latencies of P100 and N70 for the peripheral stimulation were 6 and 8 ms less than that for the central stimulation. This implies that the latency may not be sensitive to the change of SF in the fovea. Moreover, we found that the intensities of the M70 and M100 components were strongest to the high SF, especially under the pulse paradigm. The dipole analyses showed that the M70 did not yield good fits for many of the subjects under the stimuli of steady-pedestal paradigm but it did well under the stimuli of pulse paradigm. Thus, it is suggested that the M70 component might be a clue of the P-pathway when its intensities become pronounced under the pulse paradigm, whereas the M100 component was not specific to either pathway. This fact coincided with parts of the report of Proverbio et al. (1996) which pointed out that the extra-striate magnocellular source is responsible for the P95 component and the striate parvocellular source for the N70 component. As reported by Dacey (1993) in human isolated retina, they concluded that parvo-ganglion cells provide the majority of inputs from the central fovea. This may explain why the M100 component in the fovea reveals nearly negligible sensitivity to the stimulus.

Oscillatory activity associated with brain function was noted decades ago. There are three main types: (1) steady-state responses that are a natural resonance of the brain; (2) induced responses that are time- but not phase-locked to the stimulus; and (3) evoked responses that are phase-locked to the stimulus. In contrast to induced oscillatory responses, evoked responses are found to be more robust and easy to discern visually and computationally in a general experiment. In an EEG study, Tzelepi et al. (2000) demonstrated that, in response to visual stimulation, subbands of time-locked oscillatory brain waves have different functional properties. Their results showed the alpha range response reached its maximum at the P100 peak. They also suggested that the beta range was coupled to N70 and depended on SF, whereas the gamma range (34–51 Hz) was linked to the foveal processing. In our results, the alpha activity was enhanced to the low SF stimulated by steady-pedestal paradigm and to the high SF stimulated by pulse paradigm. Although no significant difference was found between different SFs, it may imply that the alpha oscillations are associated with the ascending sensory information in each pathway. This suggestion echoes the report of Schürmann and Basar (1994) which pointed out that in the human brain analysis, there is a large 10-Hz alpha response to visual stimulation in the occipital cortex. In the beta band, the power was sensitive to high SF within 0–124 ms under steady-pedestal paradigm. Furthermore, rhythmic 19–25 Hz activity was enhanced to the high SF at 100 ms under the pulse paradigm. We suggest that the beta oscillations are related to high SF which may serve for more detailed visual information. In the gamma band, we found that the power was only sensitive to the onset of the high SF stimulus under the pulse paradigm. Moreover, it seems that the gamma oscillations are involved in the signal processing of P-pathway at the fovea. Some discrepancies between

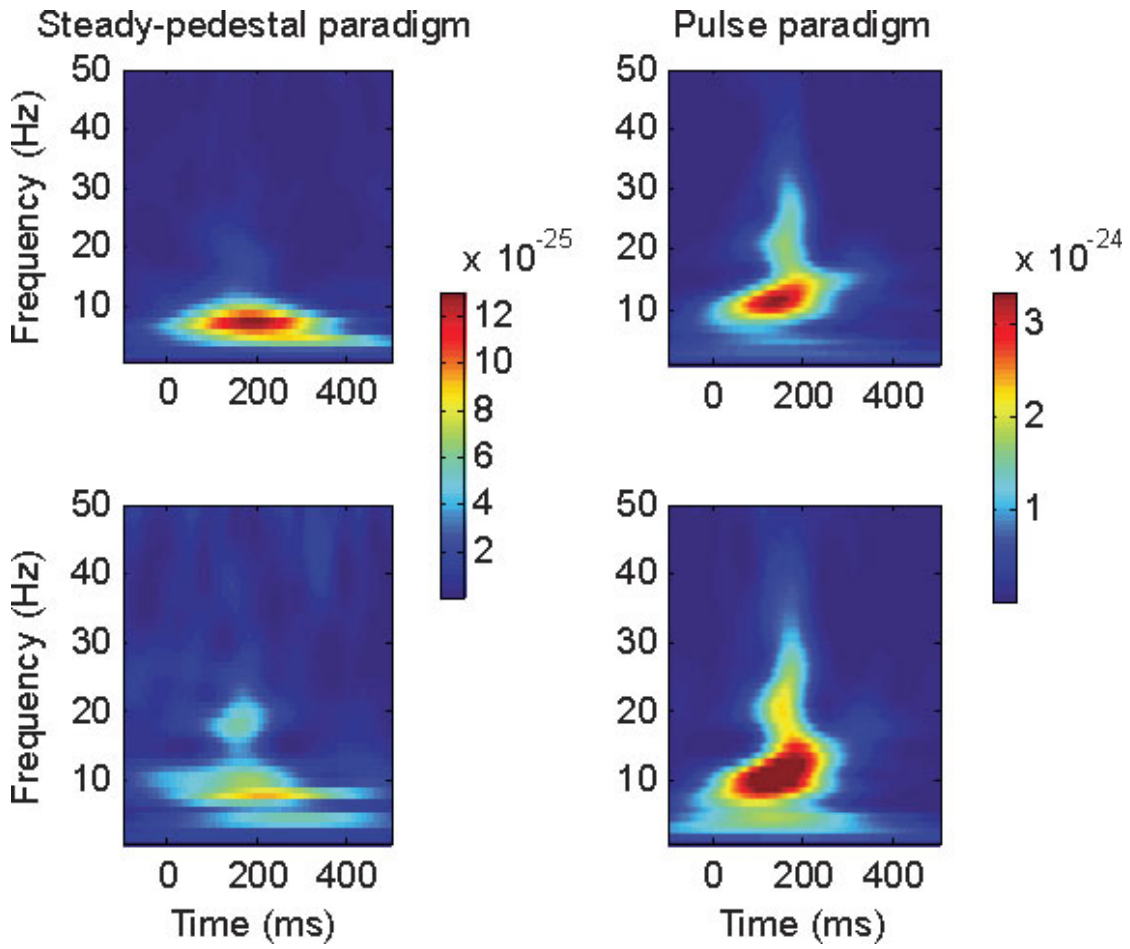

Fig. 4. Time-frequency representation of the magnetic responses over the occipital area from Subject 3 to different SFs in steady-pedestal (**left**) and pulse paradigms (**right**). The upper panels are responses to the low SF; the lower ones are responses to the high SF. The magnitude of spectral power (T^2/cm^2) from low to high is indicated with colors from blue to red.

the findings of Tzelepi et al. (2000) and our own, exhibited in the subbands of oscillatory waves, may be due to methodological differences. In their study, the signals were obtained from five electrodes in the occipital area. That number of electrode was insufficient to give reliable conclusions, not only because the spatial resolution was insufficient but also because the EEG signals could be smeared by the media below the electrodes. In addition, their visual stimulation did not aim to different pathways and

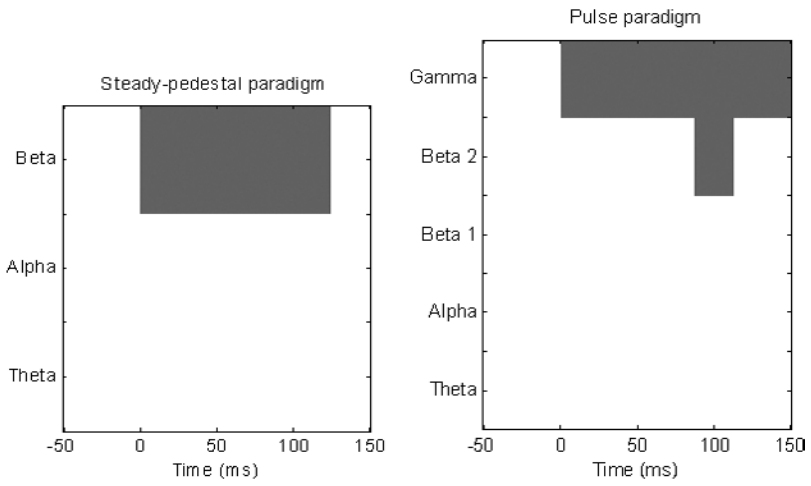

Fig. 5. Significance of the power between theta, alpha, beta, and gamma bands at each point in time. Steady-pedestal paradigm (**left**) and pulse paradigm (**right**). Red color on the plot implies significance ($p < 0.05$) using the nonparametric Wilcoxon matched-pairs signed-rank test. (Under the steady-pedestal paradigm, three frequency bands were evaluated: 3–6 Hz for theta, 7–12 Hz for alpha and 13–25 Hz for beta; under the pulse paradigm, five frequency bands were evaluated: 3–7 Hz for theta, 8–13 Hz for alpha, 14–18 Hz for beta 1, 19–25 Hz for beta 2, and 26–36 Hz for gamma.)

hence led to underestimation of the actual activity which would be interesting to investigate. Nevertheless, there is no solely functional role for brain oscillations. Variations of beta and gamma activities are not only restricted to perceptive, bottom-up mechanisms, but also observed during visual imagery or short-term memory maintenance (Tallon-Baudry, 2003).

In conclusion, our results of this study suggest that the M70 component might be a clue of the P-pathway, which responds mainly from the central fovea. In frequency analysis, the property of the beta oscillation may serve for more visual features but without identification. However, the gamma oscillation is noted to reflect the information processing in the P-pathway and is sensitive to the stimuli that ring the fovea.

Acknowledgments

This study was supported by research grants from National Science Council (NSC-93-2213-E010-016, Y Chang; NSC-92-92-2314-B075-095, NSC-93-2314-B075-084, J.C. Hsieh); National Health and Research Institute (NHRI-EX93-9332SI, J.C. Hsieh), and Taipei Veterans General Hospital (923721, 92348, 933561, 93322, J.C. Hsieh;), Taipei, Taiwan, Republic of China.

References

Adeli, H., Zhou, Z. & Dadmehr, N. (2003). Analysis of EEG records in an epileptic patient using wavelet transform. *Journal of Neuroscience Methods* **123**, 69–87.

Arakawa, K., Tobimatsu, S., Kato, M. & Kira, J.I. (1999). Parvocellular and magnocellular visual processing in spinocerebellar degeneration and Parkinson's disease: An event-related potential study. *Clinical Neurophysiology* **110**, 1048–1057.

Basar, E., Schürmann, M., Demiralp, T., Basar-Eroglu, C. & Ademoglu, A. (2001). Event-related oscillations are 'real brain responses'—wavelet analysis and new strategies. *International Journal of Psychophysiology* **39**, 91–127.

Baseler, H.A. & Sutter, E.E. (1997). M and P components of the VEP and their visual field distribution. *Vision Research* **37**, 675–690.

Bear, M.F., Connors, B.W. & Paradiso, M.A. (2001). *Neuroscience: Exploring the Brain*. Baltimore, MD: Lippincott Williams and Wilkins.

Dacey, D. (1993). The mosaic of midget ganglion cells in the human retina. *Journal of Neuroscience* **13**, 5334–5355.

Eckhorn, R., Frien, A., Bauer, R., Woelbern, T. & Kehr, H. (1993). High frequency (60–90 Hz) oscillations in primary visual cortex of awake monkey. *Neuroreport* **4**, 243–246.

Jones, D.C. & Blume, W.T. (2000). Pattern-evoked potential latencies from central and peripheral visual fields. *Journal of Clinical Neurophysiology* **17**, 68–76.

Karakas, S., Basar-Eroglu, C., Ozesmi, C., Kafadar, H. & Erzengin, O.U. (2001). Gamma response of the brain: A multifunctional oscillation that represents bottom-up with top-down processing. *International Journal of Psychophysiology* **39**, 137–150.

Kenemans, J.L., Baas, J.M.P., Mangun, G.R., Lijffijt, M. & Verbaten, M.N. (2000). On the processing of spatial frequencies as revealed by evoked-potential source modeling. *Clinical Neurophysiology* **111**, 1113–1123.

Kronland-Martinet, R., Morlet, J. & Grossmann, A. (1987). Analysis of sound patterns through wavelet transforms. *International Journal of Pattern Recognition and Artificial Intelligence* **1**, 273–302.

Kruse, W. & Eckhorn, R. (1996). Inhibition of sustained gamma oscillations (35–80 Hz) by fast transient responses in cat visual cortex. *Proceedings of the National Academy of Sciences USA* **93**, 6112–6117.

Lee, K.H., Williams, L.M., Breakspear, M. & Gordon, E. (2003). Synchronous gamma activity: A review and contribution to an integrative neuroscience model of schizophrenia. *Brain Research Reviews* **41**, 57–78.

Leonova, A., Pokorny, J. & Smith, V.C. (2003). Spatial frequency processing in inferred PC- and MC-pathways. *Vision Research* **43**, 2133–2139.

Merigan, W.H., Nealey, T.A. & Maunsell, J.H.R. (1993). Visual effects of lesions of cortical area V2 in macaques. *Journal of Neuroscience* **13**, 3180–3191.

Odaka, K., Imada, T., Mashiko, T. & Hayashi, M. (1996). Discrepancy between brain magnetic fields elicited by pattern and luminance stimulations in the fovea: Adequate stimulus positions and a measure of discrepancy. *Brain Topography* **8**, 309–316.

Plainis, S. & Murray, I.J. (2005). Magnocellular channel subserves the human contrast-sensitivity function. *Perception* **34**, 933–940.

Pokorny, J. & Smith, V.C. (1997). Psychophysical signatures associated with magnocellular and parvocellular pathway contrast gain. *Journal of the Optical Society of America A: Optics, Image Science, and Vision* **14**, 2477–2486.

Proverbio, A.M., Zani, A. & Avella, C. (1996). Differential activation of multiple current sources of foveal VEPs as a function of spatial frequency. *Brain Topography* **9**, 59–68.

Purves, D., Augustine, G.J., Fitzpatrick, D., Katz, L.C., LaMantia, A.S., McNamara, J.O. & Williams, S.M. (2001). *Neuroscience*. Sunderland, MA: Sinauer Associates.

Quiroga, R.Q. & Schürmann, M. (1999). Functions and sources of event-related EEG alpha oscillations studied with the Wavelet Transform. *Clinical Neurophysiology* **110**, 643–654.

Reed, J.L., Marx, M.S. & May, J.G. (1984). Spatial frequency tuning in the visual evoked potential elicited by sine-wave gratings. *Vision Research* **24**, 1057–1062.

Sakowitz, O.W., Quiroga, R.Q., Schürmann, M. & Basar, E. (2001). Bisensory stimulation increases gamma-responses over multiple cortical regions. *Cognitive Brain Research* **11**, 267–279.

Samar, V.J., Bopardikar, A., Rao, R. & Swartz, K. (1999). Wavelet analysis of neuroelectric waveforms: A conceptual tutorial. *Brain and Language* **66**, 7–60.

Schiller, P.H., Logothetis, N.K. & Charles, E.R. (1991). Parallel pathways in the visual system: Their role in perception at isoluminance. *Neuropsychologia* **29**, 433–441.

Schürmann, M. & Basar, E. (1994). Topography of alpha and theta oscillatory responses upon auditory and visual stimuli in humans. *Biological Cybernetics* **72**, 161–174.

Schwartz, S.H. (1999). *Visual Perception: A Clinical Orientation*. New York: McGraw-Hill.

Tallon-Baudry, C. (2003). Oscillatory synchrony and human visual cognition. *Journal of Physiology (Paris)* **97**, 355–363.

Tallon-Baudry, C. & Bertrand, O. (1999). Oscillatory gamma activity in humans and its role in object representation. *Trends in Cognitive Science* **3**, 151–162.

Taulu, S., Simola, J. & Kajola, M. (2005). Applications of the signal space separation method. *IEEE Transactions on Signal Processing* **53**, 3359–3372.

Tobimatsu, S., Tomoda, H. & Kato, M. (1995). Parvocellular and magnocellular contributions to visual evoked potentials in humans: Stimulation with chromatic and achromatic gratings and apparent motion. *Journal of the Neurological Sciences* **134**, 73–82.

Tzelepi, A., Bezerianos, T. & Bodis-Wollner, I. (2000). Functional properties of sub-bands of oscillatory brain waves to pattern visual stimulation in man. *Clinical Neurophysiology* **111**, 259–269.

Tzelepi, A., Ioannides, A.A. & Poghosyan, V. (2001). Early (N70m) neuromagnetic signal topography and striate and extrastriate generators following pattern onset quadrant stimulation. *NeuroImage* **13**, 702–718.

Varela, F., Lachaux, J.P., Rodriguez, E. & Martinerie, J. (2001). The brainweb: Phase synchronization and large-scale integration. *Nature Reviews Neuroscience* **2**, 229–239.

Wilson, H.R. (1978). Quantitative characterization of two types of line-spread function near the fovea. *Vision Research* **18**, 971–981.

Wilson, H.R., McFarlane, D.K. & Phillips, G.C. (1983). Spatial frequency tuning of orientation selective units estimated by oblique masking. *Vision Research* **23**, 873–882.

Yang, C.Y., Hsieh, J.C. & Chang, Y. (2006). An MEG study into the visual perception of apparent motion in depth. *Neuroscience letters* **403**, 40–45.